Research Article | Vol. 7, No. 11 | 1 Nov 2016 | BIOMEDICAL OPTICS EXPRESS 4514

Biomedical Optics EXPRESS

Subtraction-based approach for enhancing the depth sensitivity of time-resolved NIRS

DANIEL MILEJ,[1,2,*] ANDROU ABDALMALAK,[1,2] PETER MCLACHLAN,[1,2] MAMADOU DIOP,[1,2] ADAM LIEBERT,[3] AND KEITH. ST. LAWRENCE[1,2]

[1]*Department of Medical Biophysics, Western University, London, ON, Canada*
[2]*Imaging Division, Lawson Health Research Institute, London, ON, Canada*
[3]*Nalecz Institute of Biocybernetics and Biomedical Engineering, Warsaw, Poland*
[*]*dmilej@uwo.ca*

Abstract The aim of this study was to evaluate enhancing of the depth sensitivity of time-resolved near-infrared spectroscopy with a subtraction-based approach. Due to the complexity of light propagation in a heterogeneous media, and to prove the validity of the proposed method in a heterogeneous turbid media we conducted a broad analysis taking into account a number of parameters related to the method as well as various parameters of this media. The results of these experiments confirm that the depth sensitivity of the subtraction-based approach is better than classical approaches using continuous-wave or time-resolved methods. Furthermore, the results showed that the subtraction-based approach has a unique, selective sensitivity to a layer at a specific depth. *In vivo* application of the proposed method resulted in a greater magnitude of the hemodynamic changes during functional activation than with the standard approach.

OCIS codes: (160.4760) Optical properties; (170.3660) Light propagation in tissues; (170.6920) Time-resolved imaging; (170.7050) Turbid media.

References and links

1. A. Farina, A. Torricelli, I. Bargigia, L. Spinelli, R. Cubeddu, F. Foschum, M. Jäger, E. Simon, O. Fugger, A. Kienle, F. Martelli, P. Di Ninni, G. Zaccanti, D. Milej, P. Sawosz, M. Kacprzak, A. Liebert, and A. Pifferi, "In-vivo multilaboratory investigation of the optical properties of the human head," Biomed. Opt. Express **6**(7), 2609–2623 (2015).
2. F. Scholkmann, S. Kleiser, A. J. Metz, R. Zimmermann, J. Mata Pavia, U. Wolf, and M. Wolf, "A review on continuous wave functional near-infrared spectroscopy and imaging instrumentation and methodology," Neuroimage **85**(Pt 1), 6–27 (2014).
3. C. Hirth, H. Obrig, K. Villringer, A. Thiel, J. Bernarding, W. Mühlnickel, H. Flor, U. Dirnagl, and A. Villringer, "Non-invasive functional mapping of the human motor cortex using near-infrared spectroscopy," Neuroreport **7**(12), 1977–1981 (1996).
4. A. Torricelli, D. Contini, A. Pifferi, M. Caffini, R. Re, L. Zucchelli, and L. Spinelli, "Time domain functional NIRS imaging for human brain mapping," Neuroimage **85**(Pt 1), 28–50 (2014).
5. B. Montcel, R. Chabrier, and P. Poulet, "Detection of cortical activation with time-resolved diffuse optical methods," Appl. Opt. **44**(10), 1942–1947 (2005).
6. D. Milej, A. Gerega, M. Kacprzak, P. Sawosz, W. Weigl, R. Maniewski, and A. Liebert, "Time-resolved multi-channel optical system for assessment of brain oxygenation and perfusion by monitoring of diffuse reflectance and fluorescence," Opto-Electron. Rev. **22**(1), 55–67 (2014).
7. D. Milej, D. Janusek, A. Gerega, S. Wojtkiewicz, P. Sawosz, J. Treszczanowicz, W. Weigl, and A. Liebert, "Optimization of the method for assessment of brain perfusion in humans using contrast-enhanced reflectometry: multidistance time-resolved measurements," J. Biomed. Opt. **20**(10), 106013 (2015).
8. M. Diop and K. St Lawrence, "Improving the depth sensitivity of time-resolved measurements by extracting the distribution of times-of-flight," Biomed. Opt. Express **4**(3), 447–459 (2013).
9. A. Liebert, H. Wabnitz, D. Grosenick, M. Möller, R. Macdonald, and H. Rinneberg, "Evaluation of optical properties of highly scattering media by moments of distributions of times of flight of photons," Appl. Opt. **42**(28), 5785–5792 (2003).
10. J. T. Elliott, D. Milej, A. Gerega, W. Weigl, M. Diop, L. B. Morrison, T.-Y. Lee, A. Liebert, and K. St Lawrence, "Variance of time-of-flight distribution is sensitive to cerebral blood flow as demonstrated by ICG bolus-tracking measurements in adult pigs," Biomed. Opt. Express **4**(2), 206–218 (2013).

#270924 http://dx.doi.org/10.1364/BOE.7.004514
Journal © 2016 Received 20 Jul 2016; revised 13 Sep 2016; accepted 14 Sep 2016; published 7 Oct 2016

Biomedical Optics EXPRESS

11. A. Liebert, H. Wabnitz, and C. Elster, "Determination of absorption changes from moments of distributions of times of flight of photons: optimization of measurement conditions for a two-layered tissue model," J. Biomed. Opt. **17**(5), 057005 (2012).
12 R. R. Alfano, S. G. Demos, P. Galland, S. K. Gayen, Y. Guo, P. P. Ho, X. Liang, F. Liu, L. Wang, Q. Z. Wang, and W. B. Wang, "Time-resolved and nonlinear optical imaging for medical applications," *Ann. N. Y. Acad. Sci.*, vol. 838, no. 1 ADVANCES IN O, pp. 14–28, Feb. 1998.
13. J. Selb, D. K. Joseph, and D. A. Boas, "Time-gated optical system for depth-resolved functional brain imaging," J. Biomed. Opt. **11**(4), 044008 (2006).
14. N. Ducros, L. Hervé, A. Da Silva, J.-M. Dinten, F. Peyrin, L. Hervé, J.-M. Dinten, and F. Peyrin, "A comprehensive study of the use of temporal moments in time-resolved diffuse optical tomography: part I. Theoretical material," Phys. Med. Biol. **54**(23), 7089–7105 (2009).
15. D. Milej, A. Abdalmalak, D. Janusek, M. Diop, A. Liebert, and K. St Lawrence, "Time-resolved subtraction method for measuring optical properties of turbid media," Appl. Opt. **55**(7), 1507–1513 (2016).
16. G. E. Strangman, Z. Li, and Q. Zhang, "Depth sensitivity and source-detector separations for near infrared spectroscopy based on the Colin27 brain template," PLoS One **8**(8), e66319 (2013).
17. J. Selb, J. J. Stott, M. A. Franceschini, A. G. Sorensen, and D. A. Boas, "Improved sensitivity to cerebral hemodynamics during brain activation with a time-gated optical system: analytical model and experimental validation," J. Biomed. Opt. **10**(1), 011013 (2005).
18. A. Liebert, H. Wabnitz, N. Zołek, and R. Macdonald, "Monte Carlo algorithm for efficient simulation of time-resolved fluorescence in layered turbid media," Opt. Express **16**(17), 13188–13202 (2008).
19. D. Milej, A. Gerega, H. Wabnitz, and A. Liebert, "A Monte Carlo study of fluorescence generation probability in a two-layered tissue model," Phys. Med. Biol. **59**(6), 1407–1424 (2014).
20. A. Liebert, H. Wabnitz, J. Steinbrink, H. Obrig, M. Möller, R. Macdonald, A. Villringer, and H. Rinneberg, "Time-resolved multidistance near-infrared spectroscopy of the adult head: intracerebral and extracerebral absorption changes from moments of distribution of times of flight of photons," Appl. Opt. **43**(15), 3037–3047 (2004).
21. H. Wabnitz, A. Jelzow, M. Mazurenka, O. Steinkellner, R. Macdonald, D. Milej, N. Żołek, M. Kacprzak, P. Sawosz, R. Maniewski, A. Liebert, S. Magazov, J. Hebden, F. Martelli, P. Di Ninni, G. Zaccanti, A. Torricelli, D. Contini, R. Re, L. Zucchelli, L. Spinelli, R. Cubeddu, and A. Pifferi, "Performance assessment of time-domain optical brain imagers, part 2: nEUROPt protocol," J. Biomed. Opt. **19**(8), 086012 (2014).
22. L. Spinelli, M. Botwicz, N. Zolek, M. Kacprzak, D. Milej, P. Sawosz, A. Liebert, U. Weigel, T. Durduran, F. Foschum, A. Kienle, F. Baribeau, S. Leclair, J.-P. Bouchard, I. Noiseux, P. Gallant, O. Mermut, A. Farina, A. Pifferi, A. Torricelli, R. Cubeddu, H.-C. H.-C. Ho, M. Mazurenka, H. Wabnitz, K. Klauenberg, O. Bodnar, C. Elster, M. Bénazech-Lavoué, Y. Bérubé-Lauzière, F. Lesage, D. Khoptyar, A. A. Subash, S. Andersson-Engels, P. Di Ninni, F. Martelli, and G. Zaccanti, "Determination of reference values for optical properties of liquid phantoms based on Intralipid and India ink," Biomed. Opt. Express **5**(7), 2037–2053 (2014).
23. K. Verdecchia, M. Diop, A. Lee, and K. St. Lawrence, "Characterization of a hybrid diffuse correlation spectroscopy and time-resolved near-infrared spectroscopy system for real-time monitoring of cerebral blood flow and oxygenation," Proc. SPIE **9313**, 931310 (2015).
24. A. Abdalmalak, D. Milej, M. Diop, L. Naci, A. M. Owen, and K. St. Lawrence, "Assessing the feasibility of time-resolved fNIRS to detect brain activity during motor imagery," Proc. SPIE **9690**, 969002 (2016).
25. M. Kacprzak, A. Liebert, P. Sawosz, N. Żolek, and R. Maniewski, "Time-resolved optical imager for assessment of cerebral oxygenation," J. Biomed. Opt. **12**(3), 034019 (2007).
26. R. Re, D. Contini, M. Turola, L. Spinelli, L. Zucchelli, M. Caffini, R. Cubeddu, and A. Torricelli, "Multi-channel medical device for time domain functional near infrared spectroscopy based on wavelength space multiplexing," Biomed. Opt. Express **4**(10), 2231–2246 (2013).
27. A. T. Eggebrecht, S. L. Ferradal, A. Robichaux-Viehoever, M. S. Hassanpour, H. Dehghani, A. Z. Snyder, T. Hershey, and J. P. Culver, "Mapping distributed brain function and networks with diffuse optical tomography," Nat. Photonics **8**(6), 448–454 (2014).
28. X. Wu, A. T. Eggebrecht, S. L. Ferradal, J. P. Culver, and H. Dehghani, "Fast and efficient image reconstruction for high density diffuse optical imaging of the human brain," Biomed. Opt. Express **6**(11), 4567–4584 (2015).
29. T. Yamada, S. Umeyama, and K. Matsuda, "Separation of fNIRS signals into functional and systemic components based on differences in hemodynamic modalities," PLoS One **7**(11), e50271 (2012).
30. L. Gagnon, M. A. Yücel, D. A. Boas, and R. J. Cooper, "Further improvement in reducing superficial contamination in NIRS using double short separation measurements," Neuroimage **85**(Pt 1), 127–135 (2014).
31. A. D. Mora, E. Martinenghi, D. Contini, A. Tosi, G. Boso, T. Durduran, S. Arridge, F. Martelli, A. Farina, A. Torricelli, and A. Pifferi, "Fast silicon photomultiplier improves signal harvesting and reduces complexity in time-domain diffuse optics," Opt. Express **23**(11), 13937–13946 (2015).
32. J. Selb, T. M. Ogden, J. Dubb, Q. Fang, and D. A. Boas, "Comparison of a layered slab and an atlas head model for Monte Carlo fitting of time-domain near-infrared spectroscopy data of the adult head," J. Biomed. Opt. **19**(1), 016010 (2014).
33. K. L. Perdue, Q. Fang, and S. G. Diamond, "Quantitative assessment of diffuse optical tomography sensitivity to the cerebral cortex using a whole-head probe," Phys. Med. Biol. **57**(10), 2857–2872 (2012).
34. I. M. Wiggins and D. E. H. Hartley, "A synchrony-dependent influence of sounds on activity in visual cortex measured using functional near-infrared spectroscopy (fNIRS)," PLoS One **10**(3), e0122862 (2015).

Biomedical Optics EXPRESS

1. Introduction

Accurate estimation of optical properties of heterogeneous tissue structures by near-infrared spectroscopy (NIRS) methods is challenging [1]. Perhaps nowhere is this better exemplified than using NIRS to measure the optical properties of brain tissue, which requires contending with significant signal contamination from superficial tissue layers (skull and scalp). Various techniques have been developed to overcome this problem. The most popular and widely used in brain applications is multi-distance continuous-wave (CW) NIRS [2]. This method is based on the assumption that depth sensitivity is proportional to source-detector (r_{SD}) separation. Consequently, signals changes that occurs in the extracerebral layers can be monitored by acquiring NIRS data with a relatively small source-detector distance (r_{SD} ≈1 cm), while data acquired at a larger distance (r_{SD} > 3 cm) will provide sensitivity to the brain. CW-NIRS is frequently used in functional NIRS (fNIRS) studies [4,5].

The most advanced NIRS method is based on the time-resolved (TR) technique, which measures the distribution of times of flight of diffusely reflected photons (DTOFs) [6,7]. Measuring the DTOF not only provides a means of separating the effects of light scatter from absorption, it also provides greater depth sensitivity since light that have only travelled through superficial layers is detected earlier than light that penetrates deeper layers [7,8]. Moment analysis is a well-established method of improving depth sensitivity and determining the optical properties from DTOFs that was first introduced by Liebert et al. [9]. The first three statistical moments of DTOFs: N – total number of photons, $<t>$ – mean time of flight and V – variance are typically calculated. Due to the positive skewness of measured DTOFs, higher moments ($<t>$, V) are more sensitive to late-arriving photons. However, even these higher moments still have significant contribution from early-arriving photons [11]. Binning methods applied to DTOFs can be used to isolate photons with longer arrival times, but this approach is prone to signal-to-noise (SNR) limitations and requires careful measurement of the instrument response function (IRF) [8,12–14].

In a previous paper we presented a subtraction method (referred to as sTR) applied to the higher moments of DTOFs measured at two source-detector distances. The original objective was to avoid the need to measure the instrument response function (IRF) when measuring the absorption coefficient [15]. Moreover, it was found that the sTR method also provided more accurate estimates of the optical properties of heterogeneous media. This is not unexpected considering that higher order statistical moments and subtraction CW measurements have both been used independently to improve depth sensitivity [4,13,16,17]. The aim of the current study was to further investigate the improved depth sensitivity provided by the sTR method. Monte Carlo simulations and tissue-mimicking phantoms were used to determine how the depth sensitivity was affected by both source-detector separation and the separation between the two detectors. For comparison, moment analysis was also applied to DTOFs acquired at each detector separately [9]. As a final demonstration, TR-NIRS data acquired from the primary motor cortex during motor activation, and the magnitudes of the oxyhemoglobin concentration increases derived from moments analysis and sTR were compared.

2. Methodology

The absorption coefficient, μ_a, of a semi-infinite turbid medium can be estimated by applying moment analysis to a DTOF measured at a given source-detector separation (herein referred to as individual moment analysis or iMA) [9]:

$$\mu_a = \frac{<t>^3}{2cV\left(<t>^2 + V\right)} \qquad (1)$$

Biomedical Optics EXPRESS

where: c refers to the speed of light in the medium. The accuracy of this approach depends on carefully measuring the instrument response function.

For the sTR method, μ_a is estimated based on the difference in the mean time of flight (∂<*t*>) and variance (∂V) calculated from two DTOFs measured at separate source–detector distances. As outlined in [15], μ_a can be determined by:

$$\mu_a = \frac{\partial < t >}{2c\partial V} \tag{2}$$

2.1 Monte-Carlo simulations

Monte Carlo (MC) simulations of heterogeneous media were conducted to assess potential applications of the sTR method and for comparison to iMA. The MC algorithm was based on Liebert et al. [18] and is described in detail elsewhere [19]. The following simulations were conducted and are illustrated in Fig. 1:

a) Depth sensitivity factors [20] to changes in μ_a located at specific depth were generated for a semi-infinite geometry consisting of a stack of 10 layers, each with a thickness (d) of 0.2 cm (Fig. 1(a)). Initial values of the optical properties for all layers were set to $\mu_a = 0.1$ cm^{-1}, $\mu_s' = 10$ cm^{-1}, and a refractive index = 1.4. The sensitivity factors for iMA and sTR for the mean time-of-flight:

$$MTSF_{iMA} = \frac{\Delta < t >}{\mu_{a,j}}, \quad MTSF_{sTR} = \frac{\Delta\left(\partial < t >\right)}{\mu_{a,j}} \tag{3}$$

and variance:

$$VSF_{iMA} = \frac{\Delta V}{\mu_{a,j}}, \quad VSF_{sTR} = \frac{\Delta\left(\partial V\right)}{\mu_{a,j}} \tag{4}$$

were calculated [20] by increasing μ_a by 0.01 cm^{-1} in all consecutive layers j.

b) The ability of sTR to retrieve the optical properties of the bottom layer of a two-layer medium was assessed (Fig. 1(b)). Simulations were generated with initial values of $\mu_{a1} =$ 0.1 cm^{-1}, $\mu_{s1}' = 10$ cm^{-1} and $d_1 = 4.5$ cm for the upper layer; and $\mu_{a2} = 0.15$ cm^{-1}, $\mu_{s2}' = 10$ cm^{-1} and $d_2 = 5.5$ cm for the lower layer. Successive simulations were carried out while reducing the thickness of the upper layer from 4.5 cm to 0.5 cm.

c) The final set of simulations was performed to investigate the depth specificity of sTR to changes in μ_a located at specific depth, based on the concept that the sensitivity to a given layer will varying depending on the separation between the detectors (Δr_D). Simulations were conducted using a three-layer model (Fig. 1(c)) with the initial properties: $\mu_{a1} = 0.1$ cm^{-1}, $\mu_{s1}' = 10$ cm^{-1} and $d_1 = 1$ cm for the upper layer; $\mu_{a2} = 0.15$ cm^{-1}, $\mu_{s2}' = 10$ cm^{-1} and $d_2 = 0.5$ cm for the middle layer; and $\mu_{a3} = 0.1$ cm^{-1}, $\mu_{s3}' = 10$ cm^{-1} and $d_3 = 1$ m - (d_1 + d_2) for the lower layer. Simulations were repeated for $d_2 = 1$ and 1.5 cm.

Biomedical Optics EXPRESS

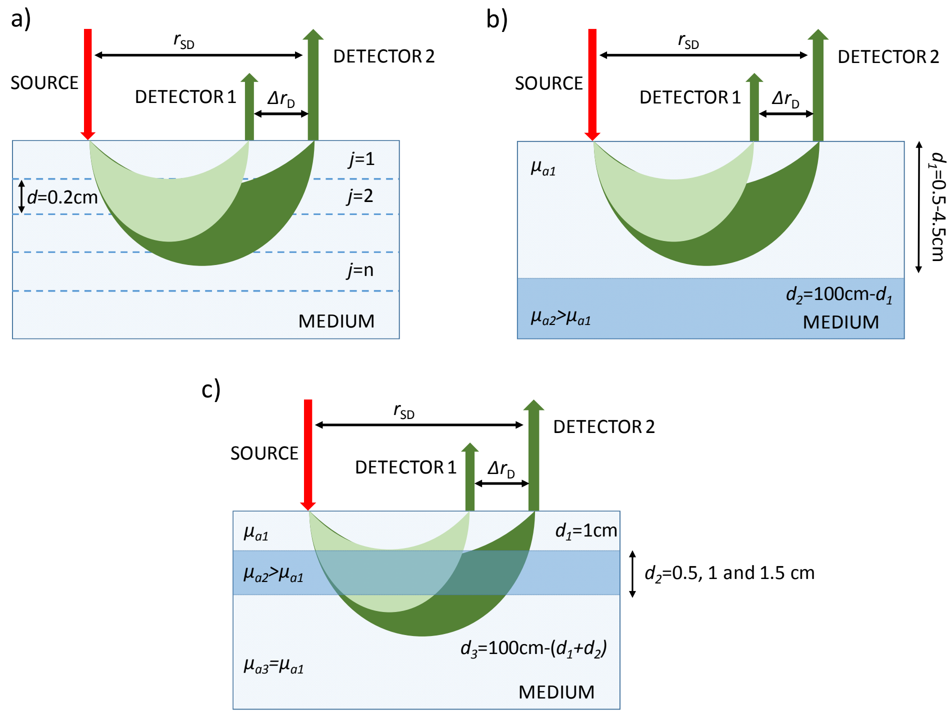

Fig. 1. Schemes for the MC simulations to assess the depth sensitivity of sTR: (a) Semi-infinite, multilayered model to generate the sensitivity factors, (b) Semi-infinite, two-layered model used to assess the sensitivity to the bottom layer, and (c) Semi-infinite, three-layered model to assess depth discrimination.

For each of the scenarios illustrated in Fig. 1, a total of $3{\cdot}10^9$ photon packages were simulated. Simulation for a single scenario took approximately an hour on a 12-core 3.4 GHz PC. DTOFs of the diffusely reflected photons were analyzed by calculation of their statistical moments.

2.2 Phantom experiments

To verify the predictions of the MC simulations, experiments were conducted with a liquid phantom with a volume of ~3 dm^3 (17.5 x 17.5 x 9 cm). The phantom included two removable membranes made of Mylar film that were used to create two and three-layered models. The phantom layers were filled with solution of water, diffusively scattering component Intralipid-20% (Fresenius Kabi AG, Germany) with a small amount of absorber (Indian Ink) added. The optical properties of the solutions were estimated using procedure proposed and validated in previous studies [21,22].

Data were acquired with a time-resolved system consisting of a picosecond pulsed diode laser (λ = 803 nm, repetition rate = 80 MHz, LDH-P-C series, PicoQuant, Berlin Germany), and two hybrid photomultiplier detectors (PMA Hybrid, PicoQuant, Berlin, Germany) coupled to a multichannel picosecond event timer and a time-correlated single photon counting (TCSPC) module (HydraHarp 400, PicoQuant, Berlin, Germany) [23]. Experiments were carried out with one emission fiber (ϕ = 400 µm, N.A. = 0.22, Fiberoptics Technology, Pomfret, CT, United States) and two custom-made fiber bundles for collection (length = 2 m, N.A. = 0.22, core 200 µm, and 3.6 mm active area; FiberTech Optica, Kitchner, ON, Canada). The optodes were positioned on the surface of the phantom using an in-house 3D printed holder, which provided a range of r_{SD} values from 1 to 6 cm. The integration time for each measurement was 60 s (i.e., a series of 200 DTOF's were obtained with an acquisition time = 300 ms).

For the experiments involving the two-layer model the initial optical properties of the phantom were: $\mu_{a1} = \mu_{a2} = 0.1$ cm^{-1} and $\mu_{s1}' = \mu_{s2}' = 10$ cm^{-1}, with a 1 cm thick top layer (d_l). Specific amounts of ink were then added to each layer separately to alter their absorption coefficients [22]: first μ_{a1} was varied between 0.1 and 0.25 cm^{-1}, then μ_{a2} was varied 0.15 to 0.35 cm^{-1}. In a second set of experiments, μ_{a1} and μ_{s1}' were set to 0.1 and 10 cm^{-1}, respectively, and μ_{a2} and μ_{s2}' were 0.15 and 10 cm^{-1}, respectively. Successive measurements were then collected while increasing the thickness of the upper layer from 0.5 cm to 4.5 cm. All experiments were conducted with two source-detector separations r_{SD} = 3 and 3.5 cm, typical of *in vivo* studies.

For the three-layered model, the initial optical properties of the Intralipid solutions were $\mu_{a1} = 0.1$ cm^{-1}, $\mu_{a2} = 0.15$ cm^{-1}, $\mu_{a3} = 0.1$ cm^{-1}, and all μ_s' values set to 10 cm^{-1}. The initial thicknesses of the top, middle and bottom layers were 0.5, 1 and 7 cm, respectively. DTOFs were acquired from the two detectors at seven r_{D2} values (0.5 to 4 cm) with $\Delta r_D = 0.5$ cm. The experiment was repeated with the thickness of the top layer increased to 1, 1.5 and 2 cm.

2.3 In vivo study

Data were acquired with the TR-NIRS system described above but modified for activation studies [24]. This consisted of two laser diodes (LDs) operating at λ = 760 nm and 830 nm. Laser pulses from both LDs were coupled into one emission fiber. The system was also equipped with two detection channels, which were built with the same optical and mechanical elements in order to ensure same IRF for the both channels. The detection fiber bundles were placed perpendicular at a distance of 3 and 4 cm with respect to the emission fiber over the left primary motor cortex as based the 10-10 international system for EEG. Three healthy subjects were recruited (male, mean age 31, right handed). The experimental paradigm consisted of five 30-s alternating periods of finger tapping (right hand) and rest to measure the oxygenation change during motor activation. The TR-NIRS data were used to calculated the changes in μ_a as a function of time from the statistical moments of the DTOFs for each detection channel separately (i.e., the iMA method) [25] and by combining the two channels for the sTR method [15]. The μ_a change measured at the two wavelengths were combined to determine the change in ΔHbO2 concentration using published values of the extinction coefficient at 760 and 830 nm. Finally, the contrast-to-noise ratio (CNR) parameter was calculated as the difference between the ΔHbO_2 value during task and rest periods divided by the standard deviation of ΔHbO_2 in the rest periods.

3. Results

3.1 Monte-Carlo simulations

The sensitivity factors derived for sTR are presented in Fig. 2 along with the corresponding sensitivity factors from iMA. Sensitivity factors were generated according to the model shown in Fig. 1(a) by shifting the depth of the perturbation layer (i.e., the 0.2 cm thick layer with the greater μ_a value) from 0.2 cm (j = 2) to 1.2 cm (j = 6). These simulations demonstrate that for a given layer, the sTR method provides greater sensitivity at a shorter source-detector separation compared to that achieved by moment analysis of individual DTOFs. The sensitivity factors for sTR also had a more selective (i.e., narrower) profile compared to iMA. Finally, the separation between the maxima of the sensitivity factors for sTR and iMA increased as the depth of the perturbation layer was increased.

Biomedical Optics EXPRESS

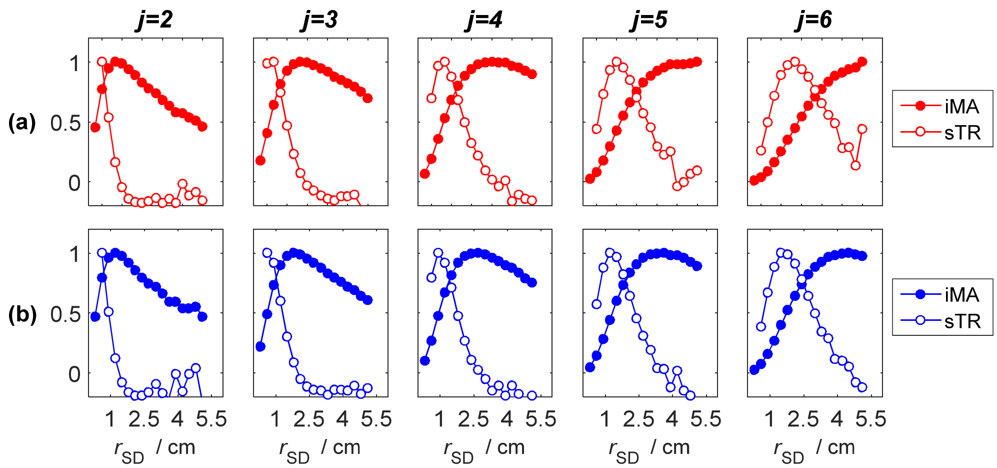

Fig. 2. Normalized sensitivity factors for (a) mean time-of-flight (*MTSF)* and (b) variance (*VSF)*. Data are presented for individual layers, denoted by *j*, of a 10-layer model plotted as a function of source-detector separation. Sensitivity factors were calculated for individual DTOFs (filled circles) and using the moment subtraction approach (open circles, Δr_D = 0.3 cm).

To further illustrate the enhanced depth sensitivity of the sTR method, the normalized sensitivity factors calculated at 4 source-detector separations (r_{SD} = 1, 2, 3 and 4 cm) are plotted in Fig. 3 as a function of depth of the perturbation layer. It can be observed that for a given r_{SD} value, the sTR method is more sensitive to deeper layers than iMA. Furthermore, the difference between the two approaches increases as r_{SD} increases.

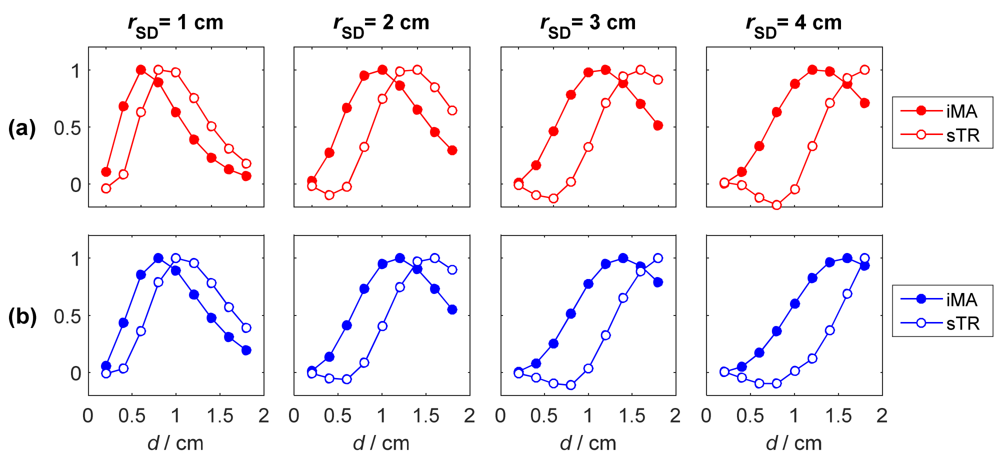

Fig. 3. Sensitivity factors for (a) mean time-of-flight and (b) variance at 4 source-detector separations. The data are presented for the moments of the DTOFs acquired at r_{SD} (filled circles) and the subtraction of two moments obtained from DTOFS separated by Δr_D = 0.5 cm (open circles). Each curve was normalized to its maximum value.

Results of the estimation of μ_a of the bottom layer of a two-layer model obtained from the MC simulations are presented in Fig. 4. In this figure, μ_a values derived from moment analysis are shown as the thickness of the upper layer (d_1) varied from 0.5 to 4.5 cm (shown in Fig. 1(b)). The sTR and iMA methods were applied to DTOFs generated for r_{SD} values of 3 and 3.5 cm – for the former, Δr_D was 0.5 cm in both cases. Both methods were able to retrieve the μ_a value of the bottom layer when $d_1 \leq 1$ cm and, conversely, the estimated μ_a values converged to the upper layer value for $d_1 > 3$ cm. The greater values of μ_a from sTR compared to those from iMA for d_1 values between 1.5 to 3 cm demonstrate its greater depth sensitivity, which is reflected by the slower convergence to μ_a for the upper layer.

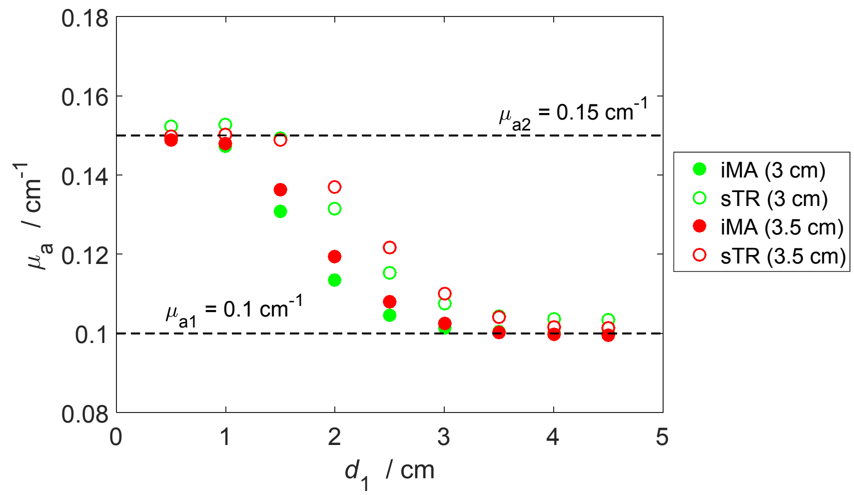

Fig. 4. Comparison of μ_a values derived from moment analysis of individual DTOFs (filled circles) and the moment subtraction method (open circles). The calculations were carried out for the model presented in Fig. 1(b) for r_{SD} = 3 cm (green symbols) and r_{SD} = 3.5 cm (red symbols) with Δr_D = 0.5 cm for the sTR method. The true values of μ_a for the upper (μ_{a1}) and lower (μ_{a2}) layers were 0.1 and 0.15 cm^{-1}, respectively.

The results of the estimation of μ_a of the middle layer of a three-layer model (shown in Fig. 1(c)) obtained from the MC simulations are presented in Fig. 5. Estimates of μ_a of the middle layer were obtained for three different values of d_2 (0.5, 1.0 and 1.5 cm), which was located at a fixed depth of 1 cm from the top surface, and for the source-detector separations given in Table 1. Photon bundles were collected simultaneously in a set of concentric, consecutive, ring-shaped detectors with fixed width.

Table 1. Configuration of the source-detector positions used in the three-layer MC simulations

	iMA		sTR		
Detector width	r_{SD}	No. of SD pairs	Detector separation (Δr_D)	r_{SD}	No. of SD pairs
0.3 cm	0.3-6 cm	20	0.3 cm	0.6-6 cm	19
0.5 cm	0.5-6 cm	12	0.5 cm	1-6 cm	11

Because of its greater depth selectivity, the sTR method was able to extract the correct μ_a value of the middle layer at shorter r_{SD} values (< 2 cm) even when the thickness of the middle layer was only 0.5 cm (Fig. 5(a)). In contrast, μ_a estimates from the iMA method (Fig. 5(b)) were always in between the input values for the middle (0.15 cm^{-1}) and the other two layers (0.10 cm^{-1}), indicating that the method remained sensitive to all layers.

Biomedical Optics EXPRESS

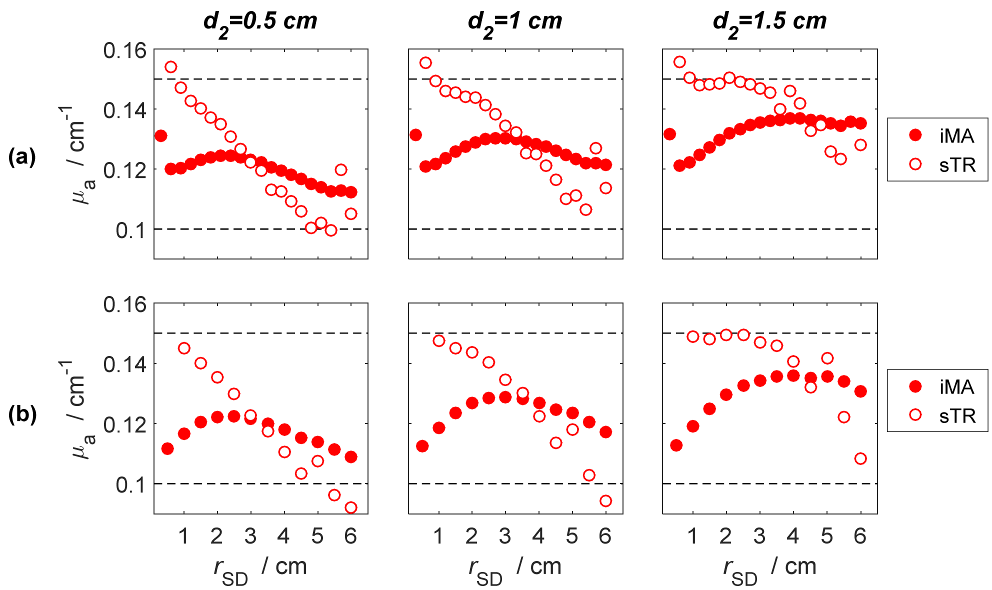

Fig. 5. Comparison of the spatial sensitivity of the moment analysis of individual DTOFs (filed circles) and the moment subtraction method (open circles). The calculations were carried out for (a) $\Delta r_D = 0.3$ cm and (b) $\Delta r_D = 0.5$ cm. Results are presented for three different thicknesses of the middle layer ($d_2 = 0.5$-1.5 cm) located at fixed depth 1 cm from the surface of the model and for the source-detector separations given in Table 1. In all simulations μ_a was 0.15 cm^{-1} for the middle layer and 0.10 cm^{-1} for the other two layers.

3.2 Phantom experiments

The results of the estimation of μ_a of the bottom layer obtained with the two-layered phantom (Figs. 6 and 7) show similar trends to the MC simulations. For the two-layered structure (shown in Fig. 1(b)), the μ_a estimates derived by applying the sTR method to data acquired at $r_{SD} = 3.5$ cm and $\Delta r_D = 0.5$ cm were fairly insensitive to μ_a changes in the upper layer (Fig. 6(a)) and were in good agreement with the μ_a values of the bottom layer (Fig. 6(b)). The greater variability observed in the μ_a estimates at $\mu_{a1} > 0.15$ cm^{-1} was due to increased noise in the higher order statistical moments. The results presented in Fig. 4(c) confirm that sTR was able to retrieve μ_a for the bottom layer for $d_1 \leq 1.5$ cm while the iMA estimates began to diverge at $d_1 = 1$ cm. As expected from the MC simulations, estimated μ_a values from both method converged to the upper layer value for $d_1 > 3$ cm. The difference between the μ_a values estimated from the two source-detector separations observed in Fig. 6(b) can be expalined by the difference in their respective depth sensitivities. For $r_{SD} = 3$ cm, the sensitivity to the bottom layer is limited and therefore the measured μ_a value is more heavily weighted to μ_a of the upper layer. The difference between the relative weights for the two source-detector separations becomes more evident as the μ_a value for the bottom layer was increased.

Biomedical Optics EXPRESS

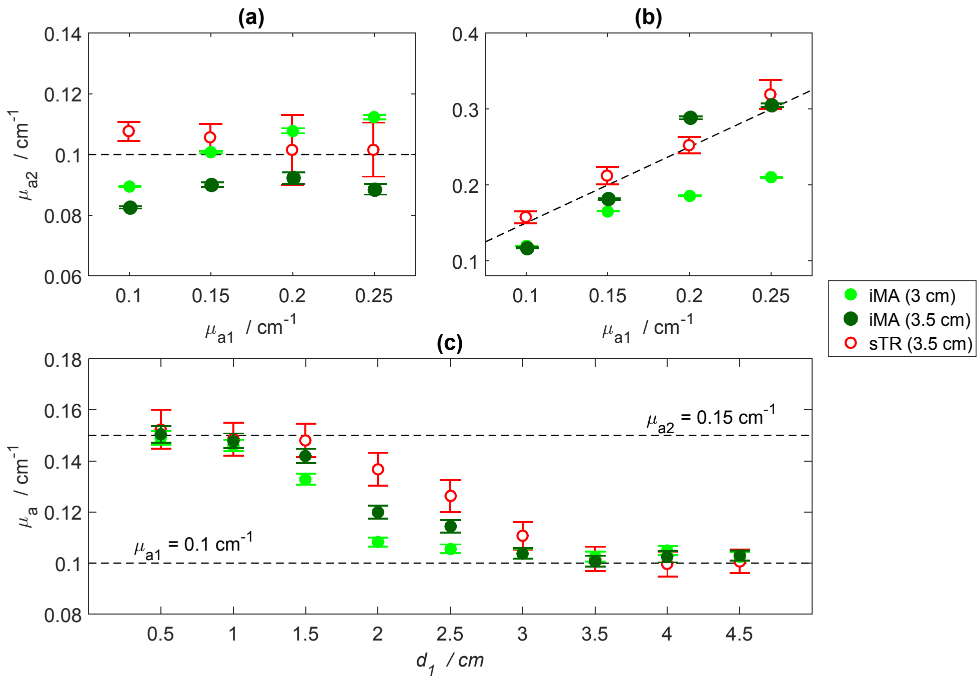

Fig. 6. Results from the two-layer phantom experiments with absorption changes in (a) the upper layer and (b) the bottom layer. (c) Comparison of μ_a values obtained from the iMA (filled circles) and sTR (open circles) methods. For the sTR method Δr_D = 0.5 cm, and the iMA method was applied to DTOFs acquired at r_{SD} = 3 cm (green), and r_{SD} = 3.5 cm (dark green). The error bars represent the standard deviation of μ_a across a series of 200 measured DTOFs.

The estimated μ_a values of the middle layer derived from the sTR and iMA methods applied to data acquired with the three-layered phantom (according to Fig. 1(c)) are presented in Fig. 7. In all cases, which spanned a range of top-layer thicknesses from 0.5 to 2 cm, the sTR method was able to retrieve the μ_a value of the middle layer. The accuracy of sTR depended on both d_1 and r_{SD}, which demonstrates the depth selectivity of the method. In contrast, the iMA method only converged to the μ_a value of the middle layer in one case (d_1 = 1.5 cm and $r_{SD} \geq$ 3.5 cm). In this case, the sTR method converged to the μ_a value of the middle layer at a shorter source-detector separation ($r_{SD} \leq$ 2 cm).

Biomedical Optics EXPRESS

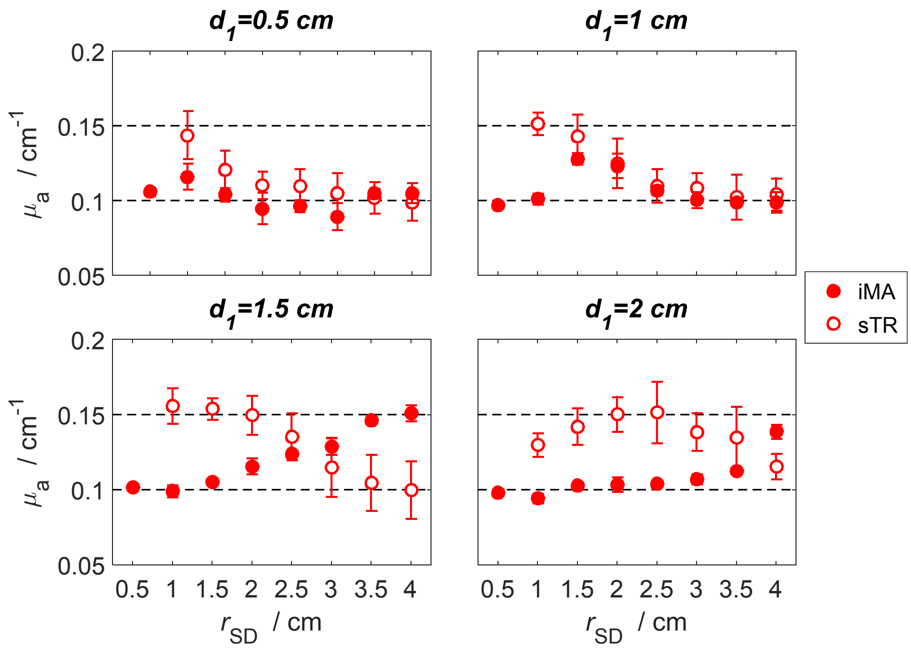

Fig. 7. Results obtained with the three-layered phantom carried out over a range of thicknesses for the top layer (d_1 = 0.5 - 2 cm). Estimated μ_a values were obtained with the sTR method (open circles) and the iMA method (filled circles). In all cases, μ_a was 0.15 cm^{-1} for the middle layer and 0.10 cm^{-1} for the other two layers. The thickness of the middle layer was 1 cm in all cases. The error bars represent standard deviation of μ_a across a series of 200 measured DTOFs.

3.3 In vivo study

The results of the *in vivo* studies confirmed the enhanced depth sensitivity of the sTR method predicted by the MC simulations and demonstrated with the tissue-phantom experiments. In all three subjects, the sTR method provided a greater change in oxyhemoglobin concentration (ΔHbO_2) during finger tapping than obtained by analyzing the DTOFs acquired at r_{SD} of 3 and 4 cm individually by the iMA method (Fig. 8). The maximum ΔHbO_2 was calculated from the mean value between 75 and 125 s relative to the mean baseline value. This signal improvement is similar to that obtained by selecting late time gates [17,26]. It should be noted that the contrast-to-noise ratio (CNR) of the sTR method appeared to be lower than the iMA approach, although this did not reach significance.

Biomedical Optics EXPRESS

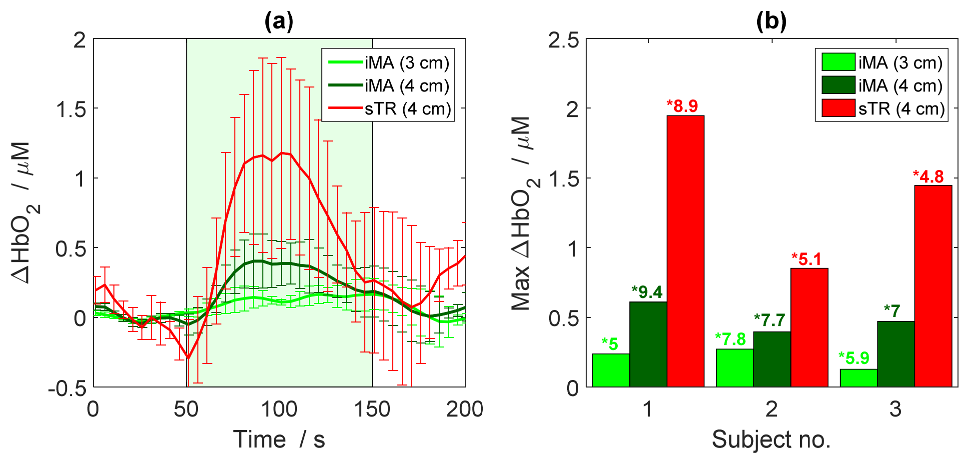

Fig. 8. (a) Increase in oxyhemoglobin concentration (ΔHbO_2) during motor activation determined by iMA applied to each r_{SD} separately (green lines) and by sTR. Time courses are the average across three subjects. The green box represents the stimulation period. (b) Magnitude of the ΔHbO_2 for each subject calculated by the iMA and sTR techniques. The CNR of each time course is indicated beside an asterisk (*). The error bars represent the standard deviation of ΔHbO_2 across subjects.

4. Discussion

Real-time *in vivo* assessment of tissue optical properties is one of the crucial advantages of NIRS, particularly for bedside monitoring of brain function. One of the limitations of NIRS for *in vivo* studies is its limited spatial resolution. This can be overcome using high-density NIRS systems [27,28] based on signals acquired at multiple source-detector distances. However, signals recorded by such systems require rigorous analysis in order to adequately separate scalp and brain signals. To overcome this issue and enhance the sensitivity of NIRS to deeper tissues (i.e., brain), TR methodology has been proposed. It has been previously shown that the sensitivity to deeper tissue can be improved by analyzing the measured DTOFs in terms of higher order statistical moments. The sTR method proposed in an earlier study [15] and applied here is based on maximizing depth sensitivity by combining higher order moment analysis with DTOFs acquired at separate source-detector distances.

The results obtained for the first group of simulations (Figs. 2 and 3) demonstrate that application of the sTR technique increases sensitivity to changes in μ_a located at specific depth at any given source-detector separation. That is, the peak of the sensitivity profile for sTR shifts toward shorter source-detector separations in comparison to the iMA approach. This feature is important because generally greater depth sensitivity is only achieved by increasing the source-detector separation [7], but at the cost of reducing CNR due to lower photon counts. The sTR technique can potentially overcome this limitation since it allows monitoring of deeper tissue compartments with the use of shorter (~2 cm) source-detector separations than iMA approach (~4 cm).

The second set of MC simulations and corresponding phantom experiments (Figs. 4 and 6) focused on evaluating the effectiveness of sTR for detecting absorption changes at greater depths in a turbid medium. The results showed that sTR provide a better response to absorption changes within the medium (for the shorter source-detector separations). Results presented in Fig. 4 shows that sTR is still able to accurately estimate μ_a at a depth of 1.5 cm. In contrast, the iMA applied to DTOFs at a source-detector distance of 3.5 cm underestimates μ_a by 15%. This advantage could be used in future studies as it can potentially prove the usefulness of the sTR technique as a tool for early detection of deeper lesions resulting from stroke or traumatic brain injury. The observed ability of the sTR method for direct

Biomedical Optics EXPRESS

measurements of the deeper tissue compartments (e.g., cerebral cortex) can be crucial for CBF monitoring since skull thickness is typically between 1 to 1.5 cm in adults. It should be also pointed out that the results of the MC simulations as well as the phantom experiments prove that the sTR method for r_{SD} >2 cm is almost insensitive to the superficial layer, which is important in neurophysiological experiments because it provide methodology for elimination of the of systemic contamination [29,30].

The final set of phantom experiments was conducted with different combinations of source-detector distances (r_{SD}) and detector separations (Δr_D) to assess the depth specificity of sTR; that is, the ability to determine μ_a accurately for a specific optical layer at a given depth and thickness. The enhanced depth specificity provided by sTR is demonstrated by the greater range of μ_a estimates shown in Figs. 5 and 7 as the depth and thickness of the target layer was varied. Figure 7 demonstrates that for a shallow target layer (i.e., $d_1 \leq 1$ cm), the sTR converges to the correct μ_a (0.15 cm^{-1}) for short r_{SD} values only. If this layer is relatively deep (i.e., $d_1 = 2$ cm), this μ_a value is obtained at r_{SD} values around 2.5 cm. In contrast, the iMA results did not show the same range of μ_a estimates. Instead, its estimates tended to converge to the μ_a value (0.1 cm^{-1}) of the upper and lower layers (Fig. 7), or to a weighted average of the two μ_a values if the depth of the target layer was constant and its thickness varied (Fig. 5). These results demonstrate that μ_a estimated from higher order moment analysis of a single DTOF is more sensitive to absorption properties over a range of layers compared to the sTR method. Applying the latter method to TR-NIRS data acquired at multiple source-detector distances may provide a means of resolving the different absorption properties of heterogeneous medium – particularly considering the advent of low-cost TR detectors [31].

As an initial *in vivo* demonstration of the sTR method, a TR-fNIRS experiment was conducted using a simple finger-tapping experiment and acquiring data at source-detector distances of 3 and 4 cm. The results presented in Fig. 8 show that magnitudes of changes in oxyhemoglobin concentration calculated by sTR were considerably higher for all three participants than the corresponding changes determined from the iMA method for each detector separately. Considering that the functional paradigm should elicit minimal hemoglobin changes in scalp, these results show that the sTR method is less sensitive to superficial tissue since the lower ΔHbO_2 obtained by the iMA method is likely due to greater partial-volume errors. This greater depth sensitivity would be advantageous for fNIRS paradigms that produce smaller hemoglobin changes than simple motor tasks [34]. However, the calculated CNR of the sTR method was lower than the analysis of individual DTOFs, which should be considered in future applications.

Funding

This study was supported by the operating grants from the Canadian Institutes of Health Research (CIHR), the Natural Sciences and Engineering Research Council of Canada (NSERC), and the National Institutes of Health (1ROINS082309), as well as a personnel award to K. St. Lawrence from the Heart and Stroke Foundation, Ontario Provincial Office. Involvement of A.L. was supported by the project UMO-2014/15/B/ST7/05276 “Spectral time-resolved measurements for cerebral blood flow assessment” financed by the Polish National Science Center.